2020

A conductive polymer derived N-doped carbon nanofiber supported Li2S coating layer for Li–S batteries with high mass loading

Fang Li
University of Wollongong

Chang Wu
University of Wollongong, cw085@uowmail.edu.au

Jicheng Jiang
University of Wollongong, jj325@uowmail.edu.au

Hua-Kun Liu
University of Wollongong, hua@uow.edu.au

Jiazhao Wang
University of Wollongong, jiazhao@uow.edu.au

A conductive polymer derived N-doped carbon nanofiber supported Li2S coating layer for Li–S batteries with high mass loading

Abstract

© 2020 Elsevier B.V. The commercialization of Li2S as a potential candidate for lithium-sulfur cathode material is hampered due to its low electronic conductivity, the “shuttle effect” and the initial energy barrier. In this work, nanosized Li2S particles coated carbon nanofibers are prepared via a solution-based chemical method. Benefiting from this synthetic method, a uniform Li2S layer can be obtained without any agglomeration. Due to the small size of Li2S particles, a smaller energy barrier is observed in the first charging process, which means it is easier to activate the Li2S with a smaller cut-off voltage. In addition, the carbon nanofibers as matrixes could enhance the conductivity of cathode. Moreover, to verify the potential practical application of prepared materials, Li2S cathodes with high loading amount of active materials (~3 mg cm−2) are prepared, which show excellent cycling and rate performance, delivering an initial specific capacity of 916.2 mA h g−1 at 0.1C, and 321 mA h g−1 capacity still can be reached at 2 C. This good performance can be attributed to the unique solution-based synthesis method, resulting in small and uniform Li2S particles coated on carbon nanofibers.

Disciplines

Engineering | Science and Technology Studies

Publication Details

Li, F., Wu, C., Jiang, J., Liu, H. & Wang, J. (2020). A conductive polymer derived N-doped carbon nanofiber supported Li2S coating layer for Li–S batteries with high mass loading. Journal of Alloys and Compounds, 828

A Conductive Polymer Derived N-doped Carbon Nanofiber Supported Li_2S Coating Layer for Li-S Batteries with High Mass Loading

*Fang Li[a,b], Chang Wu[a], Jicheng Jiang[a], Hua-Kun Liu[a], and Jiazhao Wang[a] **

[a] *Institute for Superconducting and Electronic Materials, University of Wollongong, Wollongong, NSW 2522, Australia*

[b] *School of Physics and Electronics, Hunan University, Changsha 410082, China*

**Correspondence address: jiazhao@uow.edu.au*

Abstract

The commercialization of Li_2S as a potential candidate for lithium-sulfur cathode material is hampered due to its low electronic conductivity, the "shuttle effect" and the initial energy barrier. In this work, nanosized Li_2S particles coated carbon nanofibers are prepared *via* a solution-based chemical method. Benefiting from this synthetic method, a uniform Li_2S layer can be obtained without any agglomeration. Due to the small size of Li_2S particles, a smaller energy barrier is observed in the first charging process, which means it is easier to activate the Li_2S with a smaller cut-off voltage. In addition, the carbon nanofibers as matrixes could enhance the conductivity of cathode. Moreover, to verify the potential practical application of prepared materials, Li_2S cathodes with high loading amount of active materials (~ 3 mg cm^{-2}) are prepared, which show excellent cycling and rate performance, delivering an initial specific capacity of 916.2 mA h g^{-1} at 0.1 C, and 321 mA h g^{-1} capacity still can be reached at 2 C. This good performance can be attributed to the unique solution-based synthesis method, resulting in small and uniform Li_2S particles coated on carbon nanofibers.

Keywords: nitrogen-doped carbon nanofiber, Li_2S cathode, high mass loading, uniform distribution, Li-S batteries.

1. Introduction

Lithium-sulfur (Li-S) batteries are promising power sources for portable devices and electric vehicles owing to their high specific capacity (1675 mAh g^{-1}) and energy density (2600 Wh kg^{-1}), as well as the low-cost of sulfur element.[1-4] However, the commercialization of Li-S batteries has been hampered by their innate nature, such as the insulating property of sulfur and Li_2S, the dissolved intermediate products and the large volume changes (80%) during cycling, which could lead to low utilization rate of active material and fast capacity fading.[5-7] Compared with sulfur, when lithium sulfide (Li_2S) was applied as cathode, the anode materials can use lithium-free materials,[8, 9] such as silicon, tin, carbon, etc., relieving the safety problems related to lithium anode. Moreover, the Li_2S undergoes volume shrinkage in the initial charge process,[10-12] which could release some voids to buffer the volume expansion, endowing the cathode materials with structural integrity during cycling.

Like S cathode, the Li_2S also has been facing many difficulties during its commercialization process,[13-15] such as insulating nature and the dissolved polysulfides, leading to low capacity and poor cycling stability. In addition, there is an activation energy barrier that needs to be overcome in the first charge process for the Li_2S cathode.[14] To deal with these obstacles, electrolyte modification, including exploring solid-state electrolyte[16-18] and introducing additives[19-21] (lithium nitrate, lithium iodide, transition-metal salts, etc.), has successfully relieved the shuttle effect, thus improving the long-term cycle performance of Li_2S cathode. In addition, great attention has been paid to synthesize nanosized Li_2S,[22-25] because the nanosized Li_2S usually possess a smaller activation energy barrier and faster reaction kinetics with higher specific capacity than the usual commercial Li_2S.[26]

At present, there are two commonly used methods to synthesize Li_2S nanoparticles due to its moisture sensitivity. One method is to ball mill large particles of Li_2S, which are commercially

available, with conductive additives; another method is to react Li_2SO_4 with carbon precursor at high-temperature (~ 900 °C). Although the synthesized Li_2S-C composites also showed promising electrochemical performance, both these methods have their own drawbacks: the ball-milling method directly uses commercial Li_2S particles combined with a conductive agent, which is expensive for the large-scale commercialization of Li_2S cathode; and the high-temperature method requires complicated facilities and procedures, which are not suited to large-scale production. In addition, with the solid-state reaction methods, it is usually hard to achieve a uniform Li_2S particle distribution on conductive agents. Given all these considerations, solution-based synthetic methods usually can yield small size and uniform particle distributions compared with the above-mentioned methods.[27] For example, Li_2S spheres with a uniform size of 0.5 μm can be synthesized by the solution-based chemical lithiation of S;[28] some other advanced Li_2S-carbon composites, including carbon nanotube (CNT)-Li_2S, graphene-Li_2S, and C-Li_2S have been obtained by the simple infiltration of Li_2S-ethanol solutions,[29, 30] which all showed a uniform distribution of Li_2S nanoparticles in these composites. Therefore, it is necessary to find a facile method to synthesize nanosized Li_2S and realize the uniform distribution of Li_2S on conductive matrices simultaneously.

To improve the cycling performance of Li_2S cathode, the Li_2S particles should be combined with some kinds of conductive materials (e.g. carbonaceous materials, polymer composites or conductive metal-based materials) to physically or chemically trap the polysulfides.[31-37] Among them, heteroatom-doped carbon materials have been drawn much attention due to the relative strong chemical bond between heteroatom functional groups and polysulfides, which could effectively trap the dissolved polysulfides.[38-40] For example, Yu's group designed a nitrogen and phosphorus co-doped carbon framework to support Li_2S nanoparticles for Li-S batteries,[25] which indicated that the doped nitrogen and phosphorus in the carbon could mitigate the "shuttle effect" because the heteroatoms could chemically bonded with the

polysulfides, leading to stable cycling capability. Meanwhile, heteroatom maybe help to catalyze the conversion of Li_2S into polysulfides and vice versa, improving the reaction kinetics and rate capability. Therefore, using chemical adsorbents to trap dissolved polysulfides is essential to obtain advanced Li_2S cathodes.

In this paper, a facile and solution-based synthetic method was designed to prepare Li_2S nanoparticles, which coated on the N-doped carbon nanofibers derived from polypyrrole. Due to the solution-based procedures, the Li_2S layer was uniformly coated on the carbon framework without any aggregation. The small-sized Li_2S possesses relatively lower activation barriers and could shorten the lithium-ion diffusion distance, resulting in fast kinetics for the reactions and high specific capacity. In addition, using the N-doped carbon nanofiber as the matrix could efficiently enhance the conductivity of cathode and trap soluble polysulfides, thus improving the utilization of Li_2S. Moreover, Li_2S electrode with ~ 3 mg cm^{-2} loading amount was also obtained, which deliver high capacity (705 mA h g^{-1} at 0.2 C) and good cycling stability (479.3 mA h g^{-1} can be achieved after 200 cycles at 0.2 C).

2. Experimental sections

2.1 Preparation of N-doped carbon (N-C) nanofibers

The N-C nanofibers were synthesized by thermal treatment of polypyrrole (PPy) nanofibers, which was prepared *via* a chemical oxidative polymerization process, which is detailed discussed in our previous paper.[41] The prepared PPy nanofibers were heated at 600 °C for 2 h under Ar atmosphere with a heating rate of 5 °C min^{-1} to get the N-C nanofibers.

2.2 Synthesis of sulfur coated N-C nanofibers (S@N-C)

15 mg N-C nanofiber was added into 1 mL toluene solution containing 30 mg sulfur at 60 °C, and then the raw S/N-C nanofiber was obtained after evaporating the toluene at 80 °C for 10

hours. To realize the uniform dispersion of S on the N-doped carbon nanofibers, the raw S/N-C nanofibers were sealed and reacted at 155 ºC for 10 hours in an autoclave.

2.3 Synthesis of lithium sulfide coated N-C nanofibers (Li_2S@N-C)

50 mg of the obtained S@N-C nanofibers and a certain amount of n-Butyllithium was put into a small vial with a cap and then heated to 110 °C for 4 h. After that, the obtained black powders were the Li_2S coated N-C nanofibers (denoted as Li_2S@N-C). Since the Li_2S was very sensitive to moisture, the whole process was conducted in a glovebox filled with argon and the content of H_2O and O_2 both < 0.1 ppm.

2.4 Physical Characterizations

X-ray diffraction (XRD, GBC MMA 017) were conducted to know the crystalline structure of prepared samples with a 2θ range from 10° to 80°. The field emission scanning electron microscopy (JEOL: FESEM-7500) and transmission electron microscopy (TEM, JEM-2100UHR, JEOL) were used to investigate the morphologies of the prepared composites. Due to the sensitive nature of Li_2S, the loading amount of Li_2S on N-doped carbon nanofibers was calculated by the amount of sulfur on N-C nanofibers. The loading amount of sulfur on the N-C nanofibers can be measured by Thermogravimetric analysis (TGA) using a SETARAM instrument in argon atmosphere.

2.5 Electrochemical measurements

The electrochemical performance of the Li_2S@N-C composite was investigated using 2032 coin cells, which were assembled in a glovebox with the contents of H_2O and O2 < 0.1 ppm. For preparing the Li_2S@N-C electrode, 80 wt% Li_2S@N-C hybrid, 10 wt% carbon black and 10 wt% poly(vinylidene fluoride) (PVDF) binder were mixed in N-methyl-2-pyrrolidinone (NMP) solvent to get a slurry, which was spread on the Al foil disks using a doctor blade. The

obtained electrodes were dried in glovebox for overnight at 60 °C. The pure Li_2S electrode was also prepared using the same method, which contains 55 % commercial Li_2S, 35 % carbon black and 10 % PVDF. The commercial Li_2S and carbon black were purchaded from Sigma-Aldrich with purity both > 99.95 %. The SEM images of Li_2S and carbon black are shown in Figure S2. The mass loading of Li_2S on the electrodes could be adjusted from 1 to 3 mg cm^{-2} by repeating the spread method. 1 M lithium bis(trifluoromethane sulfonyl)imide (LiTFSI) in 1,3-dioxolane (DOL)/1,2-dimethoxyethane (DME) (1:1 by volume) with 0.1 M $LiNO_3$ as additive was used as electrolyte. The cyclic voltammetry (CV) profiles were conducted using a Biologic VMP3 electrochemical workstation between 1.7 V and 2.8 V with a scan rate of 0.05 mV s^{-1}. The cycling and rate performance were obtained in a LAND battery test system at different C rates (1 C = 1166 mA g^{-1}) between 1.7 V and 2.8 V.

3. Results and Discussion

The preparation illustration for the Li_2S@N-C nanofibers is shown in **Figure 1**. First, the PPy nanofibers were prepared via a polymerization method.[41] Then, the N-doped carbon nanofibers were obtained by a thermal treatment of PPy nanofibers at 600 °C for 2 h. After that, the sulfur layer was coated on the N-doped carbon nanofibers by simple evaporation of S-toluene solution followed by vacuum redistribution. Finally, the S@N-C nanofiber was lithiated by n-Butyllithium at 110 °C for 4 h in a glove box to obtain Li_2S@N-C nanofibers.

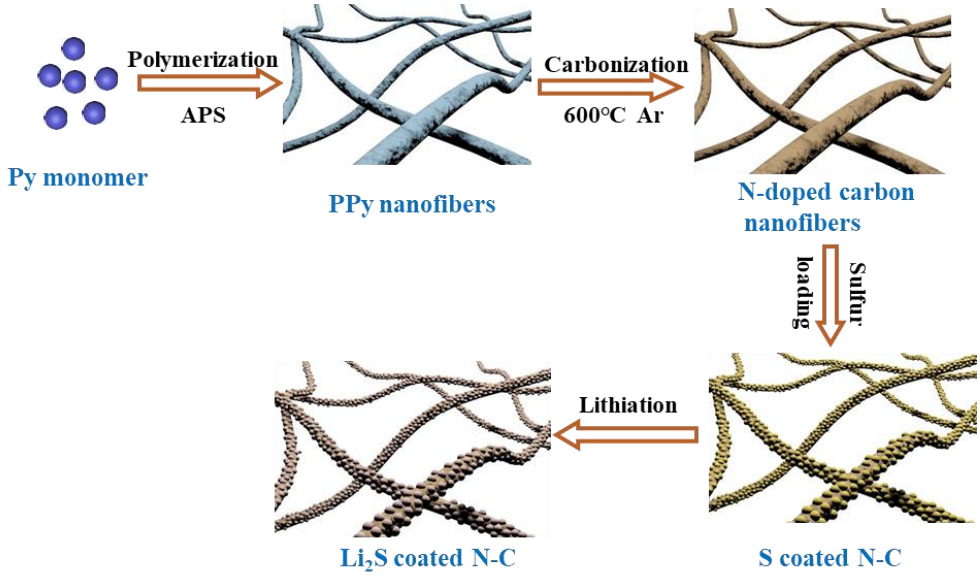

Figure 1. Schematic illustration of the preparation of the Li_2S@N-C nanofibers.

Field emission scanning electron microscope (FESEM) images were used to investigate the morphologies of the synthesized composites. **Figure 2**a shows the SEM images of the obtained PPy nanofibers with a diameter of about 70 nm. After the thermal treatment, the N-doped carbon nanofibers preserve the original morphology of the PPy nanofibers, but the surfaces of the N-doped carbon nanofibers become rougher, because during the high-temperature process, the PPy nanofiber could release lots of gas and generate many pores, obtaining a porous structure (Figure 2b), which can be able to increase the surface area to load sulfur feasibly. The S@N-C nanofiber composite still maintains this original nanofiber morphology after S loading, but a smooth surface instead of the rough one was observed, indicating an S layer coated on the N-C nanofibers (Figure 2c). Figure 2d shows SEM images of Li_2S@N-C nanofibers, which show the same morphology as the S@N-C nanofibers, and there is no obvious agglomeration of nanoparticles, indicating the uniform distribution of Li_2S on the surfaces of the N-C nanofibers. The structural characterization of the Li_2S@N-C nanofibers was also determined by the Transmission electron microscopy (TEM) images. As shown in Figure 2e, the Li_2S@N-

C nanofibers maintain the fibrous structure of the S@N-C nanofibers, which is consistent with the SEM image (Figure 2d). High-Resolution TEM (HRTEM) reveals that Li_2S nanoparticles show a very small size (less than 5 nm), which are tightly embedded in the N-doped porous carbon nanofibers. The corresponding elemental maps further confirm the carbon, nitrogen, and sulfur elements were homogeneous distribution in the Li_2S@N-C nanofibers (Figure 2g), indicating the uniform distribution of Li_2S on the N-C nanofibers.

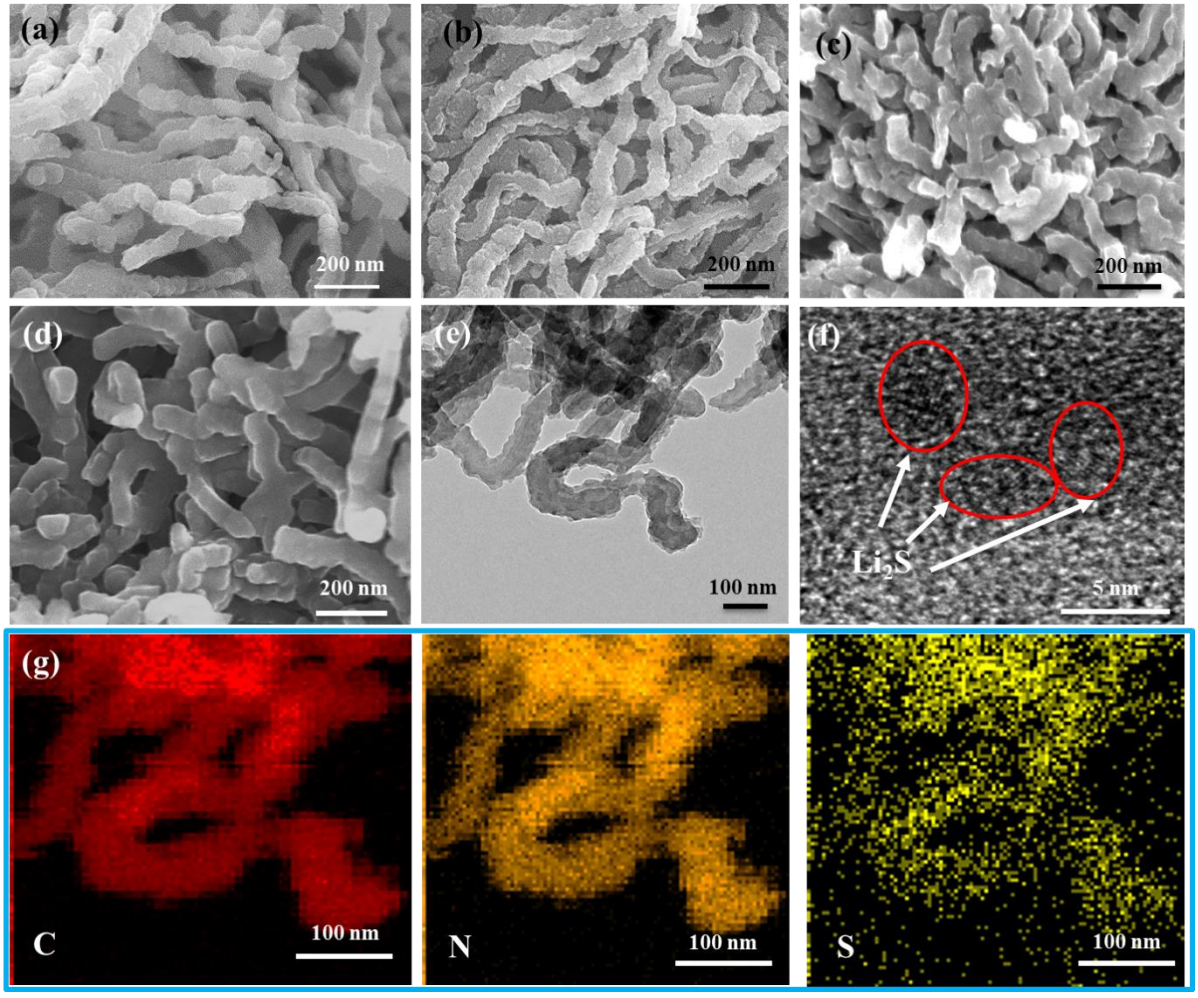

Figure 2. SEM images of (a) PPy nanofibers, (b) N-doped carbon nanofibers, (c) S@N-C nanofibers, and (d) Li_2S@N-C nanofibers, (e) TEM and (f) HRTEM images of Li_2S@N-C nanofibers, and (g) corresponding element mapping.

X-ray diffraction (XRD) patterns were used to confirm the crystalline structures of the prepared composites, as shown in **Figure 3**a. The N-doped carbon nanofibers possess an amorphous structure by showing a broad peak between 20-30°. And the pronounced peaks in the S@N-C sample belongs to the orthorhombic sulfur (JCPDS card No: 08-0427). After reaction with n-Butyllithium, sulfur is converted into cubic phase Li_2S (JCPDS card No. 77-2145). No sulfur residual and other crystal impurity were observed, indicating the complete conversion of sulfur to Li_2S. Raman spectroscopy was applied to further prove the successful synthesis of Li_2S in the composite, as shown in Figure 3b. For pure Li_2S, the peak located at 372 cm^{-1} is related to the T_{2g} phonon mode of Li_2S, representing the Li-S bond vibrations.[33, 42] The N-C nanofibers show two peaks at around 1355 cm^{-1} and 1597 cm^{-1}, which is related to the D band and the G band, respectively.[43] The Raman spectrum of the Li_2S@N-C nanofibers shows the characteristic peaks of both Li_2S and N-doped carbon, indicating the successful loading of Li_2S on N-C nanofibers, which is consistent with the results of element mapping (Figure 2g). The amount of sulfur coated on the S@N-C composite was investigated by the Thermogravimetric analysis (TGA) in pure argon atmospheres. Because the Li_2S was obtained from the lithiation of sulfur, the content of Li_2S coated on the N-C nanofibers can be calculated from the content of sulfur. As shown in Figure 3c, the sulfur in the S@N-C composites is 64%, which means that the Li_2S amount coated on the surface of N-C nanofibers is 68%.

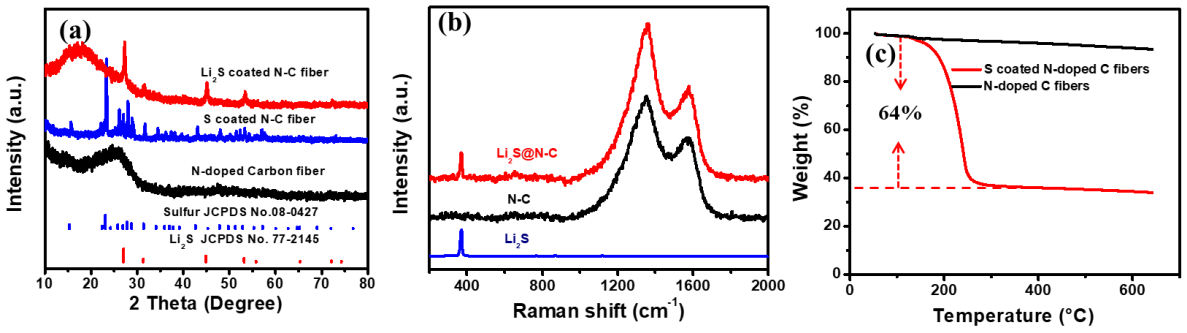

Figure 3. (a) XRD patterns of prepared N-doped carbon nanofibers, S@N-C nanofibers, and Li_2S@N-C nanofibers; (b) Raman spectra of commercial Li_2S, N-doped carbon nanofibers, and Li_2S@N-C nanofibers; (c) TGA curves of N-doped carbon nanofibers, S@N-C nanofibers in Ar atmosphere.

The electrochemical performances of the synthesized Li_2S@N-C hybrid and commercial Li_2S particles were first investigated by cyclic voltammetry (CV) measurements, which were shown in **Figure 4**a and b. Due to the energy barrier in the first charging process, the electrodes were first activated by charging to 4 V.[15] From Figure 4a and b, the Li_2S@N-C and pure Li_2S electrodes both show one typical anodic peak and two typical cathodic peaks. The first reduction peak located at ~ 2.3 V can be ascribed to the conversion of sulfur to long-chain polysulfides (Li_2S_n, $2 < n \leqslant 8$), which is soluble in the electrolyte and results in "shuttle" effect. Then the long-chain polysulfides will be further reduced to lithium sulfides (Li_2S_2/Li_2S), which is revealed by the second cathodic peak located at around 2.0 V. The peak at around 2.5 V in the oxidation process represents the conversion of Li_2S to Li_2S_n ($2 < n \leqslant 8$), and finally to S.[44] The Li_2S@N-C electrode shows an additional small oxidation peak at ~ 3.5 V in the initial charging process, however, which is related to the energy barrier needed to activate the Li_2S cathode. The pure Li_2S electrode also shows a broad peak at 3.7 V in the initial charging process, as shown in Figure 4b, which is located at higher voltage position than that of the Li_2S@N-C electrode, indicating that the potential barrier of Li_2S@N-C electrode is lower than that of pure Li_2S electrode, owing to the small size and uniform distribution of the prepared Li_2S particles on the N-C nanofibers.[15, 45] After the first activation, these electrodes both can normally work in the following cycles just like sulfur cathode, which means that the Li_2S electrode was successfully activated by the high cut-off voltage.

The charge-discharge profiles of Li_2S@N-C and pure Li_2S electrodes are also shown in Figure 4c and d. For the Li_2S@N-C electrode, the cut-off voltage was set to 3.6 V, while for the pure

Li_2S electrode, the cut-off voltage was set to 4 V. As we can see, in the first charging process, the voltage rapidly increased and then decreased, followed by a gradual increase to the cut-off voltage. The voltage increase at the beginning is known as the energy barrier of Li_2S.[46] The energy barrier of Li_2S@N-C electrode is slightly lower than that of the pure Li_2S electrode. After activation, the charge-discharge profiles of Li_2S@N-C and pure Li_2S electrode both show two discharge plateaus, relating to the reduction of sulfur to long-chain lithium polysulfides, and then to the lithium sulfides (Li_2S_2/Li_2S). The discharge plateaus are long and flat, indicating a stable out-put power can be achieved. In the charging process, there is one plateau, which was related to the reversible reaction from Li_2S to sulfur. These results are all consistent with the CV results. The above results indicate that a cut-off voltage of 3.6 V is enough for Li_2S@N-C electrode to activate Li_2S due to the small size and uniform distribution of the as-prepared Li_2S. The activation voltage of this work compared with some related papers, which is listed at Table S1. The activation voltage of 3.6 V is smaller than most of that of published works.

The cycling performance of Li_2S@N-C and pure Li_2S electrode with Li_2S mass loading of 1 mg cm^{-2} are also compared in **Figure 6a**. The electrode was firstly cycled for 10 cycles at 0.1 C to fully activate the Li_2S, and then cycled at 0.2 C. The Li_2S@N-C electrode shows a much higher specific capacity than that of pure Li_2S electrode in the whole cycling process. The pure Li_2S electrode delivered an initial discharge capacity of 1017.3 mA h g^{-1} at 0.1 C and decreased to 550.5 mA h g^{-1} after 20 cycles at 0.2 C, showing a fast capacity fading. Compared to pure Li_2S electrode, the Li_2S@N-C electrode experiences a more stable cycling capability, delivering an initial specific capacity of 1036.6 mA h g^{-1} at 0.1 C and maintaining at a capacity of 704.2 mA h g^{-1} after 200 cycles. The results of this work compared with some reported literatures, which is listed in Table S2. The prepared Li_2S@N-C materials show better electrochemical performance than many related Li_2S composites. From the above results, the cycling capability of Li_2S@N-C electrode is visibly enhanced compared with the pure Li_2S

electrode, suggesting that the N-C nanofibers could efficiently adsorb lithium polysulfides, mitigating the shuttle effect of intermediate products. In addition, the small size and uniform distribution of Li_2S particles could improve the utilization of Li_2S.

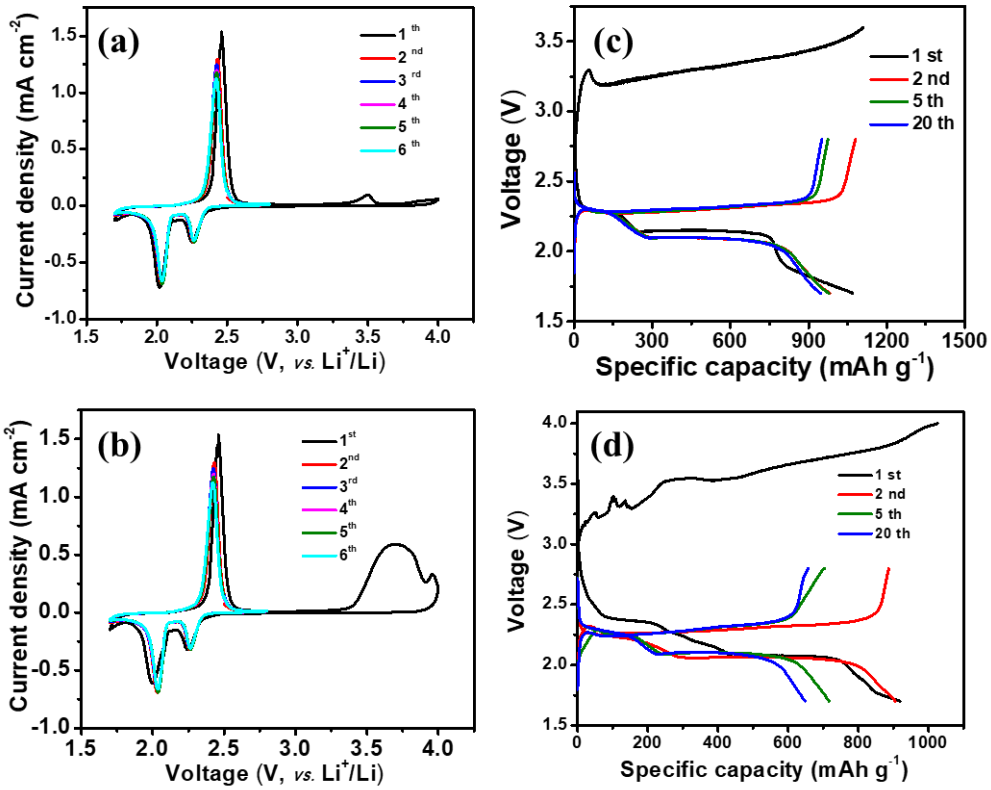

Figure 4. CV profiles of (a) Li_2S@N-C and (b) pure Li_2S at 0.05 mV s^{-1}; Charge-discharge profiles of (c) Li_2S@N-C and (d) pure Li_2S electrodes at different current densities.

To investigate the effect of prepared eelctrode on trapping polysulfides during the cycling process, the cycled Li_2S@N-C and pure Li_2S electrodes at a fully charged stage were disassembled after 50 cycles. The cycled electrodes were put into a dioxolane/dimethoxyethane (DOL/DME) (v/v = 1:1) solvent for 12 h. Then, ultraviolet-visible (UV-vis) spectroscopy is conducted to measure the amount of soluble polysulfides dissolved in the electrodes. After 12 h soak, the colour of DOL/DME solutions with different cycled electrodes were shown in the inset of **Figure 5** using digital photographs. The colour of DOL/DME solutions with cycled

Li_2S@N-C electrode is lighter yellow, while the colour of DOL/DME solutions with cycled pure Li_2S electrode is dark yellow, indicating less polysulfides were dissolved into electrolyte in the Li_2S@N-C electrode. The UV-vis absorption spectra of the above-mentioned solutions were shown in Figure 5. The adsorption peak of Li_2S@N-C electrode is lower than that of the pure Li_2S electrode, indicating the Li_2S@N-C electrode could efficiently anchor the polysulfides and reduce their dissolution compared with that of pure Li_2S electrode, resulting a high utilization rate of active materials and stable cycling performance.

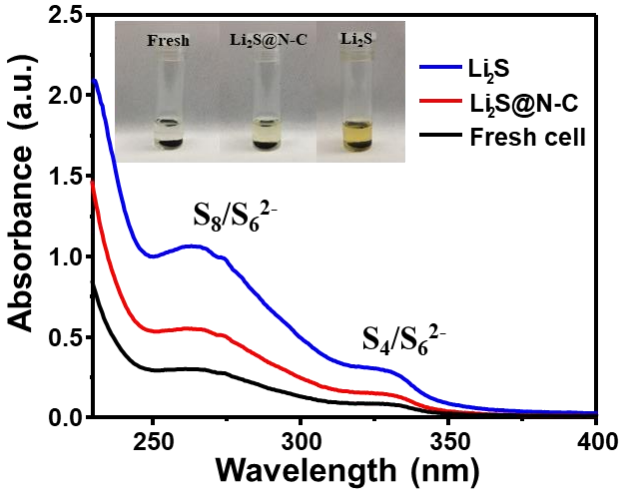

Figure 5. UV/vis absorption spectra of DOL/DME solutions exposed to cycled Li_2S@N-C and pure Li_2S electrodes after 50 cycles, with the inset showing the colour of the solutions exposed to different electrodes.

For practical application, the large loading mass of active materials is very important. The Li_2S@N-C cathodes with different loading mass of 1, 2, and 3 mg cm^{-2} were evaluated, as shown in **Figure 6**a. The electrodes were first fully activated for 10 cycles at 0.1 C, and then cycled for 200 cycles at 0.2 C. As we can see, the specific capacities are decreasing with increasing Li_2S loading. The Li_2S@N-C composite with a mass loading of 1 mg cm^{-2} delivers the highest initial specific discharge capacity of 1036.6 mA h g^{-1} at 0.2 C, and after 200 cycles a high capacity of 704.2 mA h g^{-1} is still maintained. The Li_2S@N-C composites with a mass loading of 2 mg cm^{-2} and 3 mg cm^{-2} also show a discharge capacity of 602.5 mA h g^{-1} and

479.3 mA h g^{-1}, respectively, after 200 cycles. These results indicate that the thick electrode could prevent the rapid transfer of electrons into/from the active materials and reduce the utilization of Li_2S (**Figure S1**). Nevertheless, the Li_2S@N-C electrode with 3 mg cm^{-2} active materials still shows higher specific capacity than the pure Li_2S with 1 mg cm^{-2} active materials, which can be ascribed to the small size and uniform distribution of our prepared Li_2S particles and the conductive N-C nanofibers, which both are beneficial to the fast electrons transport and enhance the use ratio of Li_2S. The rate capability of the Li_2S@N-C composites with different mass loading is shown in Figure 6b. The Li_2S@N-C composite with 1 mg cm^{-2} mass loading shows the highest capacities at all current density, which delivers a specific discharge capacity of 1106.4, 880.3, 769.6, 683.9, 571.4, and 489.3 mA h g^{-1} at 0.1 C, 0.2 C,0.3 C, 0.5 C, 1 C, and 2 C, respectively. Even at a high current density of 5 C, the specific capacity still can reach 380.4 mA h g^{-1}. And when the current density was suddenly recovered back to 0.1 C, a discharge capacity of 887.5 mA h g^{-1} still obtained. In comparison, the Li_2S@N-C composite with 2 mg cm^{-2} mass loading can deliver a specific discharge capacity of 233 mA h g^{-1} at 5 C. And the Li_2S@N-C composite with 3 mg cm^{-2} mass loading shows capacities of 916.2, 677, 598.1, 505.4, 376.8, 321 and 139 mA h g^{-1} at 0.1 C, 0.2 C, 0.3 C, 0.5 C, 1 C, 2 C, and 5 C, respectively. The Li_2S@N-C electrode with high mass loading shows excellent cycling and rate performance, which can be ascribed to the following reasons: First, the small size of Li_2S prepared by the solution-based method could possess a small energy barrier in the first charging process, which is easier to activate and improves the utilization; Second, the N-doped carbon could improve the conductivity of electrode and enhance the utilization of active materials.

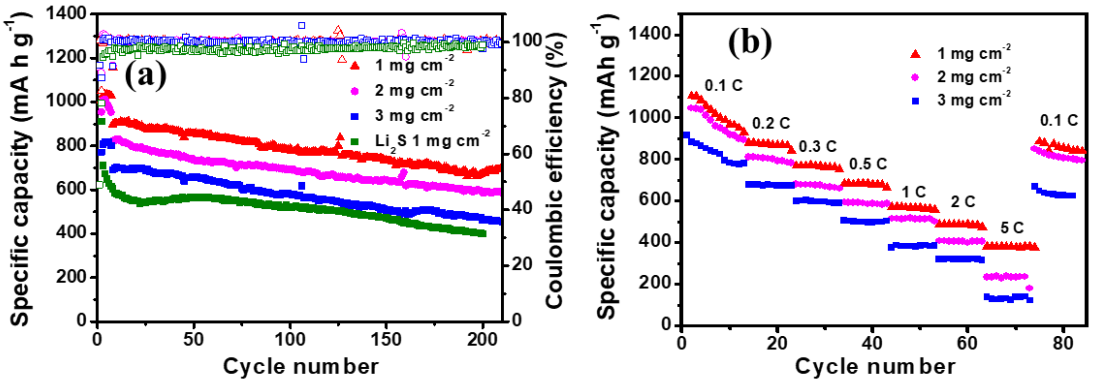

Figure 6. (a) Cycling performance and (b) rate capability of different electrodes with different mass loading of active materials.

4. Conclusion

In summary, a facile solution-based chemical method has been reported for the preparation of Li_2S@N-C composites. Compared with the solid-based method and thermal treatment method, the solution-based method could yield small-sized Li_2S particles and a uniform distribution of them on the matrix without agglomeration, which could enhance the contact between the N-C nanofibers and the Li_2S particles. The N-doped carbon nanofiber matrix derived from PPy nanofibers could enhance the electrical conductivity of electrode and improve the utilization of Li_2S. In addition, a Li_2S@N-C electrode with a 3 mg cm^{-2} loading amount was prepared to show the potential for practical application of our prepared samples, and it delivered high specific capacity of 916.2 mA h g^{-1} and 321 mA h g^{-1} at 0.1 and 2 C, which is both higher than that of pure Li_2S electrode with a 1 mg cm^{-2} loading amount. The excellent cycling stability and rate capability can be ascribed to small size and uniform distribution of Li_2S particles on the N-doped carbon nanofibers. This work is likely to be helpful and offer new insight into the preparation of nanosized Li_2S composites as a high-performing Li-S cathode material with high active material loading.

Acknowledgments

This work is supported by an Australian Research Council (ARC) Linkage Project (LP160100914). The authors would like to thank Dr. Tania Silver for critical reading of the manuscript.

References

1. A. Manthiram, Y. Fu, S.-H. Chung, C. Zu and Y.-S. Su, *Chemical Reviews*, 2014, **114**, 11751-11787.
2. Z.-L. Xu, J.-K. Kim and K. Kang, *Nano Today*, 2018, **19**, 84-107.
3. Z. W. Seh, Y. Sun, Q. Zhang and Y. Cui, *Chemical Society Reviews*, 2016, **45**, 5605-5634.
4. A. Manthiram, S. H. Chung and C. Zu, *Advanced Materials*, 2015, **27**, 1980-2006.
5. S. Rehman, K. Khan, Y. Zhao and Y. Hou, *Journal of Materials Chemistry A*, 2017, **5**, 3014-3038.
6. R. Fang, S. Zhao, Z. Sun, D. W. Wang, H. M. Cheng and F. Li, *Advanced Materials*, 2017, **29**, 1606823.
7. X. Yang, X. Li, K. Adair, H. Zhang and X. Sun, *Electrochemical Energy Reviews*, 2018, **1**, 239-293.
8. Y. Yang, M. T. McDowell, A. Jackson, J. J. Cha, S. S. Hong and Y. Cui, *Nano Letters*, 2010, **10**, 1486-1491.
9. J. Brückner, S. Thieme, F. Böttger-Hiller, I. Bauer, H. T. Grossmann, P. Strubel, H. Althues, S. Spange and S. Kaskel, *Advanced Functional Materials*, 2014, **24**, 1284-1289.
10. Y. Tsao, M. Lee, E. C. Miller, G. Gao, J. Park, S. Chen, T. Katsumata, H. Tran, L.-W. Wang and M. F. Toney, *Joule*, 2019, **3**, 872-884.
11. S. Liang, Y. Xia, C. Liang, Y. Gan, H. Huang, J. Zhang, X. Tao, W. Sun, W. Han and W. Zhang, *Journal of Materials Chemistry A*, 2018, **6**, 9906-9914.
12. X. Wang, X. Bi, S. Wang, Y. Zhang, H. Du and J. Lu, *ACS Applied Materials & Interfaces*, 2018, **10**, 16552-16560.
13. D. Su, D. Zhou, C. Wang and G. Wang, *Advanced Functional Materials*, 2018, **28**, 1800154.
14. G. Zhou, H. Tian, Y. Jin, X. Tao, B. Liu, R. Zhang, Z. W. Seh, D. Zhuo, Y. Liu and J. Sun, *Proceedings of the National Academy of Sciences USA*, 2017, **114**, 840-845.
15. Y. Yang, G. Zheng, S. Misra, J. Nelson, M. F. Toney and Y. Cui, *Journal of the American Chemical Society*, 2012, **134**, 15387-15394.
16. Q. Pang, A. Shyamsunder, B. Narayanan, C. Y. Kwok, L. A. Curtiss and L. F. Nazar, *Nature Energy*, 2018, **3**, 783.
17. R.-c. Xu, X.-h. Xia, X.-l. Wang, Y. Xia and J.-p. Tu, *Journal of Materials Chemistry A*, 2017, **5**, 2829-2834.
18. R.-c. Xu, X.-h. Xia, S.-h. Li, S.-z. Zhang, X.-l. Wang and J.-p. Tu, *Journal of Materials Chemistry A*, 2017, **5**, 6310-6317.
19. B. D. Adams, E. V. Carino, J. G. Connell, K. S. Han, R. Cao, J. Chen, J. Zheng, Q. Li, K. T. Mueller and W. A. Henderson, *Nano Energy*, 2017, **40**, 607-617.
20. G. G. Eshetu, X. Judez, C. Li, O. Bondarchuk, L. M. Rodriguez-Martinez, H. Zhang and M. Armand, *Angewandte Chemie International Edition*, 2017, **56**, 15368-15372.
21. F. Wu, J. T. Lee, N. Nitta, H. Kim, O. Borodin and G. Yushin, *Advanced Materials*, 2015, **27**, 101-108.
22. T. Yang, X. Wang, D. Wang, S. Li, D. Xie, X. Zhang, X. Xia and J. Tu, *Journal of Materials Chemistry A*, 2016, **4**, 16653-16660.
23. Y. Peng, Y. Zhang, Z. Wen, Y. Wang, Z. Chen, B.-J. Hwang and J. Zhao, *Chemical Engineering Journal*, 2018, **346**, 57-64.
24. M. Yu, Z. Wang, Y. Wang, Y. Dong and J. Qiu, *Advanced Energy Materials*, 2017, **7**, 1700018.

25. J. Zhang, Y. Shi, Y. Ding, L. Peng, W. Zhang and G. Yu, *Advanced Energy Materials*, 2017, **7**, 1602876.
26. M. R. Kaiser, X. Liang, H.-K. Liu, S.-X. Dou and J.-Z. Wang, *Carbon*, 2016, **103**, 163-171.
27. S. Y. Zheng,Y. Chen, Y. H. Xu, F. Yi, Y. J. Zhu, Y. H. Liu, J. H. Yang, C. S. Wang, *ACS Nano*, 2013, **7**, 10995-11003.
28. C. Nan, Z. Lin, H. Liao, M.-K. Song, Y. Li and E. J. Cairns, *Journal of the American Chemical Society*, 2014, **136**, 4659-4663.
29. Y. Kim, H. Han, Y. Noh, J. Bae, M. H. Ham and W. B. Kim, *ChemSusChem*, 2019, **12**, 824-829.
30. F. Wu, J. T. Lee, E. Zhao, B. Zhang and G. Yushin, *ACS Nano*, 2015, **10**, 1333-1340.
31. H. Yan, H. Wang, D. Wang, X. Li, Z. Gong and Y. Yang, *Nano Letters*, 2019, **19,** 3280-3287.
32. J. He, Y. Chen and A. Manthiram, *Advanced Energy Materials*, 2019, **9**, 1900584.
33. Z. W. Seh, H. Wang, P.-C. Hsu, Q. Zhang, W. Li, G. Zheng, H. Yao and Y. Cui, *Energy & Environmental Science*, 2014, **7**, 672-676.
34. L. Chen, Y. Liu, F. Zhang, C. Liu and L. L. Shaw, *ACS Applied Materials & Interfaces*, 2015, **7**, 25748-25756.
35. F. Wu, T. P. Pollard, E. Zhao, Y. Xiao, M. Olguin, O. Borodin and G. Yushin, *Energy & Environmental Science*, 2018, **11**, 807-817.
36. C. Chen, D. Li, L. Gao, P. P. R. Harks, R.-A. Eichel and P. H. Notten, *Journal of Materials Chemistry A*, 2017, **5**, 1428-1433.
37. M. R. Kaiser, Z. Han, J. Liang, S.-X. Dou and J. Wang, *Energy Storage Materials*, 2019, **19,** 1-15.
38. D. Su, M. Cortie and G. Wang, *Advanced Energy Materials*, 2017, **7**, 1602014.
39. Y. Xia, R. Fang, Z. Xiao, H. Huang, Y. Gan, R. Yan, X. Lu, C. Liang, J. Zhang and X. Tao, *ACS applied materials & interfaces*, 2017, **9**, 23782-23791.
40. F. Pei, T. An, J. Zang, X. Zhao, X. Fang, M. Zheng, Q. Dong and N. Zheng, *Advanced Energy Materials*, 2016, **6**, 1502539.
41. F. Li, M. R. Kaiser, J. Ma, Z. Guo, H. Liu and J. Wang, *Energy Storage Materials*, 2018, **13**, 312-322.
42. B. Bertheville, H. Bill and H. Hagemann, *Journal of Physics: Condensed Matter*, 1998, **10**, 2155.
43. J. Wang, L. Liu, S. Chou, H. Liu and J. Wang, *Journal of Materials Chemistry A*, 2017, **5**, 1462-1471.
44. R. Fang, S. Zhao, Z. Sun, D. W. Wang, H. M. Cheng and F. Li, *Advanced Materials*, 2017, **29,** 1606823.
45. J. Y. Koh, M.-S. Park, E. H. Kim, B. O. Jeong, S. Kim, K. J. Kim, J.-G. Kim, Y.-J. Kim and Y. Jung, *Journal of The Electrochemical Society*, 2014, **161**, A2133-A2137.
46. C. Zu, M. Klein and A. Manthiram, *The Journal of Physical Chemistry Letters*, 2014, **5**, 3986-3991.